Journal of the European Ceramic Society 44 (2024) 116709

Contents lists available at ScienceDirect

Journal of the European Ceramic Society

journal homepage: www.elsevier.com/locate/jeurceramsoc

Feature article

Recommended strategies for quantifying oxygen vacancies with X-ray photoelectron spectroscopy

Jiayue Wang [a,*], David N. Mueller [b], Ethan J. Crumlin [c,d,**]

[a] Geballe Laboratory for Advanced Materials, Stanford University, Stanford, CA 94305, USA
[b] Peter Grünberg Institute, Forschungszentrum Jülich, Jülich 52425, Germany
[c] Chemical Sciences Division, Lawrence Berkeley National Laboratory, Berkeley, CA 94720, USA
[d] Advanced Light Source, Lawrence Berkeley National Laboratory, Berkeley, CA 94720, USA

ARTICLE INFO

Keywords:
XPS
Ambient pressure XPS
Quantifying oxygen vacancies

ABSTRACT

Oxygen vacancies play a crucial role in shaping the properties of metal oxides for diverse applications such as catalysis, ferroelectricity, magnetism, and superconductivity. Although X-ray photoelectron spectroscopy (XPS) is a robust tool, accurate quantification of oxygen vacancies remains a challenge. A common mistake in XPS analysis is associating the 531–532 eV feature in O 1*s* spectra with oxygen vacancies. This is incorrect because a vacant oxygen site does not emit photoelectrons and therefore does not generate a direct XPS spectral feature. To address this issue, we propose three alternative approaches for oxygen vacancy analysis with XPS through *indirect* features: (1) quantifying cation valence state variations, (2) assessing oxygen nonstoichiometry via normalized oxygen spectral intensity, and (3) evaluating Fermi energy changes from electrostatic shifts in the binding energy. The recommended strategies will facilitate precise XPS analysis of oxygen vacancies, promoting future studies in understanding and manipulating oxygen vacancies for advanced material development.

1. Introduction

Metal oxides are at the forefront of materials design due to their broad applications in clean energy systems, information storage and processing, and quantum technology, among others [1–3]. The functionality and durability of these metal oxide devices depend strongly on internal atomic perturbations (i.e., point defects), particularly oxygen vacancies, which are missing atoms at the oxygen lattice sites [4–7]. Previous studies have shown that the formation and annihilation of oxygen vacancies in metal oxides can significantly affect their properties in applications such as catalysis [8], ferroelectricity [9], magnetism [10], superconductivity [11], and ionic conductivity [12]. Therefore, obtaining a better understanding of oxygen vacancies and how to control them is crucial to materials innovation for next-generation technologies.

X-ray photoelectron spectroscopy (XPS) is a powerful tool for investigating the chemistry and electronic structure of materials [13–15]. Nevertheless, accurately quantifying oxygen vacancies through XPS poses a persistent challenge. Since vacant oxygen lattice sites do not directly produce XPS signals, the selection of suitable XPS features for quantifying oxygen vacancies in materials remains controversial. To date, a commonly adopted approach in the literature is to deconvolute the O 1*s* spectra into lattice oxygen and oxygen vacancy components, with the latter typically exhibiting a binding energy between 531 eV and 532 eV [16,17]. While widely used in the literature, there is no clear physical basis for this assignment and analysis. First, it is clear that this ~531 eV feature cannot be directly generated by an oxygen vacancy, as the prerequisite for an XPS signal (the existence of an oxygen 1*s* electron) is not met at an unoccupied oxygen site. Furthermore, recent *in situ* XPS studies on CeO_2 [18] and TiO_2 [19] have shown that the O 1*s* spectral profile remains largely unchanged before and after reduction, indicating that the ~531 eV O 1*s* shoulder peak is also unlikely to originate from neighboring oxygen sites near an oxygen vacancy [20,21]. Instead, accumulating evidence [22–25] suggests that the 531–532 eV feature in the O 1*s* spectrum arises from physisorbed or chemisorbed oxygen species (e.g., hydroxyl groups) on oxide surfaces [26]. As gas molecules can preferentially adsorb onto oxygen vacancies [27], the concentrations of surface-adsorbed oxygen species and oxygen vacancies may sometimes show correlation [17,28]. However, using the features of oxygen adsorbates to quantify surface oxygen vacancy

* Corresponding author.
** Corresponding author at: Chemical Sciences Division, Lawrence Berkeley National Laboratory, Berkeley, CA 94720, USA.
E-mail addresses: jiayue@stanford.edu (J. Wang), ejcrumlin@lbl.gov (E.J. Crumlin).

https://doi.org/10.1016/j.jeurceramsoc.2024.116709
Received 9 May 2024; Received in revised form 27 June 2024; Accepted 28 June 2024
Available online 1 July 2024
0955-2219/© 2024 The Authors. Published by Elsevier Ltd. This is an open access article under the CC BY-NC-ND license (http://creativecommons.org/licenses/by-nc-nd/4.0/).

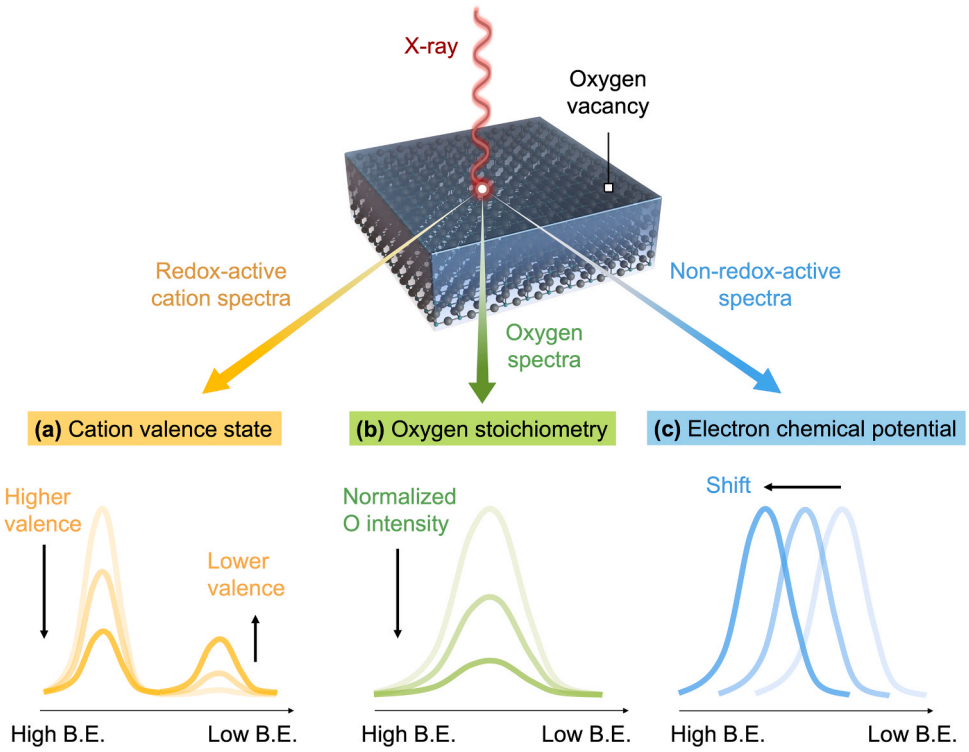

Fig. 1. The three proposed approaches for quantifying oxygen vacancies using XPS: (a) cation valence state, (b) oxygen nonstoichiometry, and (c) electron chemical potential shift.(a) In the first approach, the oxygen vacancy concentration in materials is quantified by monitoring the change in valence state of the redox-active cations, assuming charge neutrality. (b) The second approach involves quantifying the O-to-cation ratio or tracking the evolution of normalized oxygen spectral intensity. This allows for probing the oxygen nonstoichiometry in oxides. (c) The third approach investigates oxygen vacancy by monitoring the rigid shift in binding energy from redox-inert elements, which remain in a constant valence state during oxygen release reactions. This shift is attributed to the modulation of the Fermi level position in oxides resulting from oxygen vacancy formation. In all figures (a-c), the direction of the arrows indicates the formation of oxygen vacancies, i.e., lattice reduction. B.E. denotes binding energy.

concentrations is notably inaccurate. For instance, even in a fully oxidized sample, the concentration of surface adsorbed oxygen can be substantial [29–31]. Therefore, relying on the ~531 eV feature in the O 1*s* spectra to analyze oxygen vacancies is incorrect. A thorough reevaluation of the method for precise oxygen vacancy analysis in XPS is essential for the advancement of the field.

In this paper, we propose a three-fold approach to oxygen vacancy quantification with XPS, focusing on the electronic [32] and stoichiometric [33] changes induced by oxygen vacancy formation and annihilation. First, through the analysis of redox-active cations, which lower their valence states upon oxygen vacancy formation, the concentration of oxygen vacancies can be determined (Fig. 1a). Second, oxygen vacancies can be quantified by examining the surface oxygen-to-cation stoichiometry, which decreases as materials release oxygen and form oxygen vacancies (Fig. 1b). Third, due to electron doping, the electron chemical potential in oxides may increase upon oxygen vacancy formation. Consequently, XPS can be used to probe oxygen vacancies in materials by assessing shifts in the electron chemical potential within the samples (Fig. 1c). It is important to note that not all three approaches work equally well (or at all) on all materials, and thus it is important to understand the physical, chemical, and spectroscopic behavior of the materials in order to choose the right approach. In the following sections, we provide an in-depth exploration of how XPS can be used to quantitatively evaluate oxygen vacancies in different material classes using these three techniques.

2. Probing oxygen vacancies via cation valence state

When an oxide forms an oxygen vacancy, it is often accompanied by a decrease in the valence state of redox-active cations [34,35]. Under such scenarios, the presence of oxygen vacancies in materials may be deduced from the evolution of XPS cation spectra if the spectra are straightforward to interpret. This is usually the case when the reduced form of the cation has a single electron in the outermost shell, so no multiplet effects complicate the spectral shapes [36], and the electrons used to compensate for the oxygen vacancies are quite localized. In Fig. 2, we present several examples from the literature illustrating the evolution of XPS cation spectra during oxygen vacancy formation in several different materials.

In CeO_2, the oxygen vacancy formation is accompanied by the reduction of Ce^{4+} to Ce^{3+} (Ref. [37]), corresponding to a change from a $4f^0$ to a $4f^1$ configuration, which can be probed with both Ce 4*d* and valence band XPS spectra (Fig. 2a). For the Ce 4*d* spectra, the two components exhibiting the highest binding energies (as shown in the shaded region in the plot) originate from Ce^{4+} species. Notably, the Ce^{4+} features diminish as the lattice undergoes reduction, indicating a reduction in the ceria surface. Examining the valence band spectra, the feature at approximately 1.5 eV corresponds to the Ce 4*f* peak, which reflects the concentration of Ce^{3+} at the surface. Additionally, the intensity of the valence band Ce 4*f* peak increases as the surface undergoes further reduction. In TiO_2, the formation of oxygen vacancies correlates with the reduction of Ti^{4+} to Ti^{3+} ($3d^0$ to $3d^1$). Consequently, Ti^{3+} species are evident in the lower binding energy region of the Ti 2*p* spectrum for the reduced TiO_2 samples [19] (Fig. 2b). In Fig. 2c, we show the cation spectral evolution during the reduction of V_2O_5 (Ref. [38]). In the oxidized state, only V^{5+} ($3d^0$) species can be observed in the V 2*p* spectra. However, the V 2*p* spectra of reduced V_2O_5 exhibits a shoulder peak in the lower binding energy region, suggesting the formation of V^{4+} ($3d^1$). All three compounds exhibit little charge transfer from the ligand to the cation [39], so cation core-level XPS is a valid

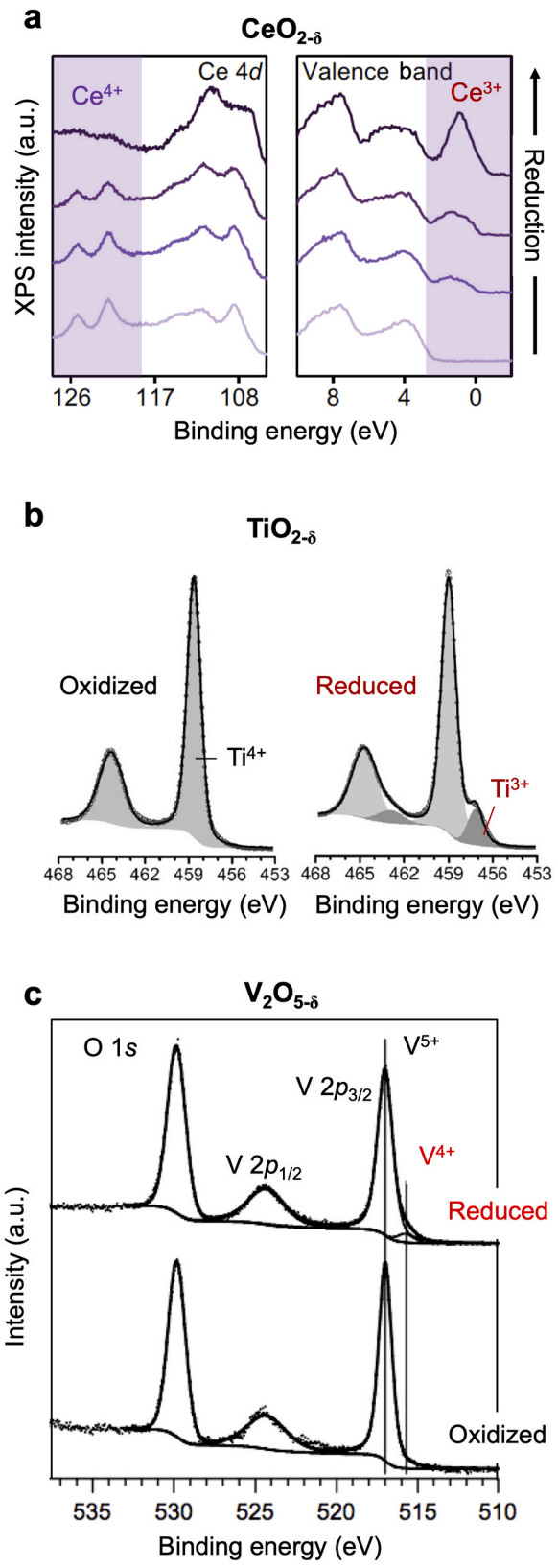

Fig. 2. Cation XPS spectral evolution during oxide reduction. (a) Ce 4*d* and valence band evolution during the reduction of CeO_2, highlighting the decrease in the Ce^{4+} feature and the concurrent increase in Ce^{3+}. (b) Ti 2*p* spectra of stoichiometric and reduced TiO_2. (c) V 2*p* spectra showing the emergence of V^{4+} species during the reduction of V_2O_5.
(a) Reproduced from Ref. [37] with permission from the Royal Society of Chemistry. (b) Reproduced with permission from Ref. [19]. (c) Reproduced with permission from Ref. [38].

probe for the valence state.

Based on the cation spectral evolution described above, the concentration of oxygen vacancies can be quantified by calculating the valence state of cations, *assuming* that charge neutrality is preserved within the probing depth of XPS and charge compensation for vacancies is exclusively electronic and not ionic by, *e.g.*, formation of interstitials or Schottky defects. For example, in the case of reduced TiO_2 shown in Fig. 2b, the concentration of Ti^{3+} was calculated to be 12 % by fitting the Ti 2*p* spectra [19]. Based on the quantified Ti^{3+} concentration, the surface composition can be calculated as $Ti^{4+}_{0.88}Ti^{3+}_{0.12}O^{2-}_{1.94}$. We can therefore calculate the oxygen nonstoichiometry for the reduced TiO_2 sample as $2 - 1.94 = 0.06$. Notably, the key aspect of this approach lies in precisely determining the valence state of cations in materials, which requires careful fitting of the XPS spectra. A comprehensive discussion on XPS fitting is beyond the scope of this review; however, interested readers can find detailed guidance in the literature (for example, Ref. [40–42]).

As discussed in the introduction, we want to emphasize that the formation of oxygen vacancies in metal oxides does not always lead to significant changes in peak shapes observed in cation XPS spectra. Consider, for example, negative charge transfer oxides such as $La_{1-x}Sr_xFeO_3$ (LSF), where the redox center primarily resides on the ligand (i.e., O). [43,44] In such cases, the formation of oxygen vacancies tends to have a negligible impact on the cation valence state, and, consequently, the peak shape in cation XPS spectra remains largely unchanged [45] as the electron configuration changes from $3d^5\underline{L}$ to $3d^5$ upon reduction, where $\underline{L}$ denotes a ligand hole [46]. Therefore, relying solely on cation spectral analysis would not be adequate for quantifying oxygen vacancies in these materials. In the following sections, we discuss a technique to quantify oxygen vacancies in such scenarios by examining oxygen nonstoichiometry and Fermi energy shift.

3. Probing oxygen vacancies via oxygen non-stoichiometry

As materials release oxygen and generate oxygen vacancies, the oxygen concentration within the oxide lattice diminishes, leading to a reduction in the intensity of lattice oxygen species in XPS spectra. Therefore, oxygen vacancies can be probed with XPS by quantifying the oxygen nonstoichiometry (δ) in oxides. Specifically, the change in surface oxygen nonstoichiometry ($\Delta\delta$) during oxygen vacancy formation relative to the oxidized surface can be determined using the following equation:

$$\Delta\delta = 1 - \frac{A(O_{lattice})}{A(O_{lattice})_{oxidized}} \quad (1)$$

where *A* denotes the lattice oxygen peak area in the *normalized* oxygen spectra (e.g., O 1*s*) and the subscript "oxidized" denotes the spectra collected on an oxidized sample surface.

We want to emphasize that in Eq. 1, it is crucial to utilize the normalized oxygen spectral intensity rather than the absolute intensity derived from the raw XPS data. This normalization is essential because the raw XPS intensity can be affected by numerous factors beyond surface oxygen stoichiometry, such as surface roughness, temperature, gas atmosphere, and photon intensity [13]. Therefore, to mitigate interference from these factors, normalizing the oxygen spectral intensity is necessary for accurately quantifying oxygen nonstoichiometry. Here, we suggest normalizing the oxygen spectra to the intensity of a redox-inert cation spectrum, which should be collected under identical environmental conditions and during the same XPS measurement. When analyzing materials that do not have redox-inert cation spectra, such as binary oxides, normalizing the oxygen spectra can also be achieved using the XPS background intensities or the area of the redox-active

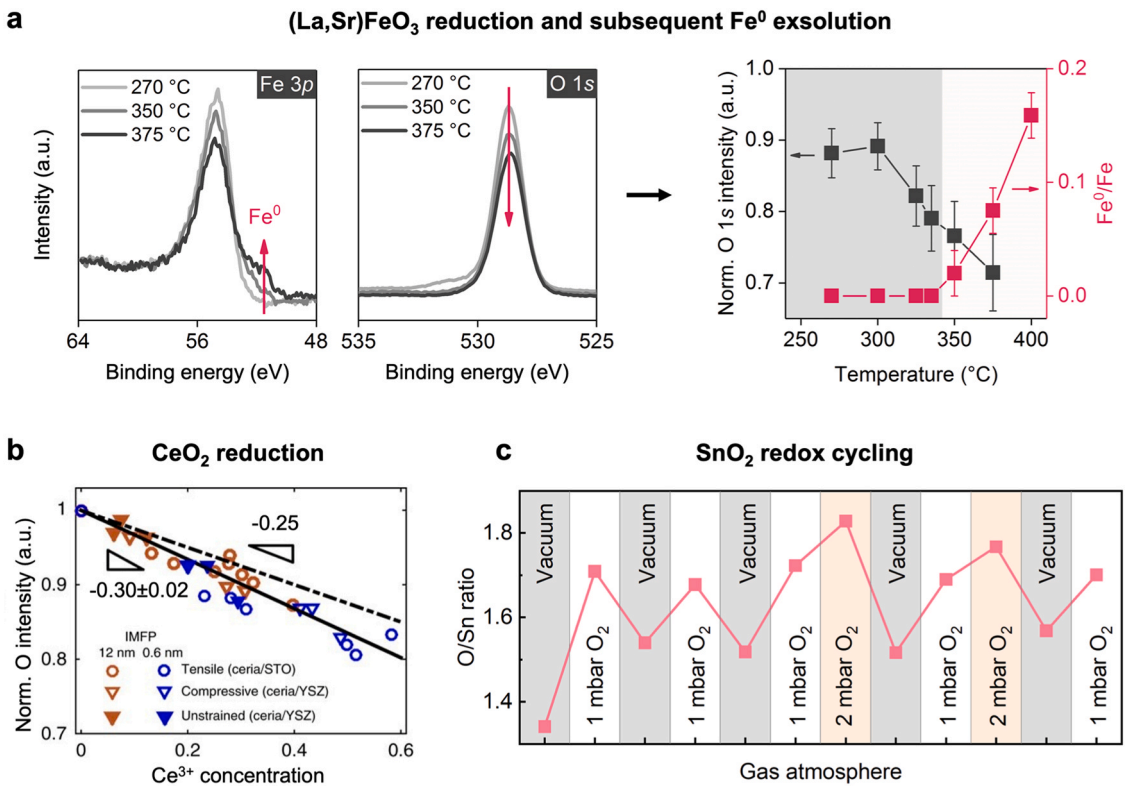

Fig. 3. Oxygen spectral intensity evolution during redox reactions.(a) *In situ* Fe 3*p* and O 1*s* spectra of $La_{0.6}Sr_{0.4}FeO_{3-\delta}$ heated an in H_2 atmosphere. The normalized O 1*s* intensity decreases during sample reduction, accompanied by the formation of reduced metallic iron (Fe^0) specie. (b) Normalized oxygen intensity decreases as the CeO_2 surface undergoes reduction. Note that the experimentally observed slope relating oxygen intensity to surface Ce^{3+} concentration is 0.30, closely matching the electroneutral site fraction of 0.25. (c) XPS quantification of the O-to-Sn ratio during the redox-cycling of $SnO_{2-\delta}$. Notably, the O/Sn ratio evolution captures surface oxidation or reduction upon changes in the gas atmosphere.
(a) Reproduced from Ref.[50] Copyright 2021 American Chemical Society (b) Reproduced from Ref. [53] with permission. (c) Reproduced from Ref. [54] with permission from the Royal Society of Chemistry.

cation spectra. Nonetheless, this approach may introduce increased uncertainty, as the normalization factor itself could fluctuate during the chemical reaction. Notably, surface oxygen vacancy formation or annihilation is sometimes linked to the emergence of surface heterogeneity, including phenomena such as cation segregation [47] and dissolution [48]. In such cases, the normalization process can become more complex and might require modeling [49]. Below, we explore several examples in Fig. 3 where normalized oxygen spectra are utilized for quantifying surface oxygen stoichiometry.

In the first example, we show normalized O 1*s* intensity can be used to quantity surface oxygen stoichiometric variation in perovskite oxides during reduction. For LSF, *in-situ* Fe 3*p* and O 1*s* spectra were collected as the sample underwent reduction during heating in an H_2 atmosphere [50] (Fig. 3a). Here, the O 1*s* spectra were normalized to the La 4*d* intensity. Notably, the normalized O 1*s* intensity begins to decrease above 300 °C, indicating that the rate of oxygen release in LSF (i.e., the formation rate of oxygen vacancies) only becomes discernible at elevated temperatures [44]. In this analysis, O 1*s* spectra were normalized to the intensity of La 4*d*, as La remains inert during the reduction reaction. Upon further heating of LSF, the oxygen intensity continues to decrease with increasing temperature, suggesting an increasing concentration of oxygen vacancies within LSF. Eventually, at temperatures exceeding 350 °C, the emergence of metallic Fe^0 species on the surface becomes evident. The Fe^0 formation represents the partial decomposition of LSF [51] because the oxygen nonstoichiometry in LSF exceeds the thermo-chemical stability limit [52] of the perovskite phase. Therefore, by analyzing both the cation and anion spectra, one can effectively probe the formation of oxygen vacancies in a dynamic phase transformation process, as demonstrated in this study.

In the second example, we show that the normalized O 1*s* and O 2*p* peaks can be used to quantify the extent of reduction of the binary oxide CeO_2 (Fig. 3b). As detailed in reference [53], the near-surface fraction of Ce^{3+} was determined using the Ce 4*f* feature in the valence-band spectra (see Fig. 2a). Moreover, the O 2*p* and O 1*s* spectra were normalized by the integrated intensity of Ce 4*d* spectra. As illustrated, the normalized oxygen intensity decreases as the sample undergoes reduction, revealing a reverse correlation with the surface Ce^{3+} concentration. Notably, the ratio between the changes in normalized O intensity and surface Ce^{3+} concentration was quantified to be 0.30±0.02, which closely aligns with the electroneutral site fraction of 0.25. This self-consistency underscores the efficacy of both the cation and anion XPS spectra in the analysis of oxygen vacancies in oxides.

As a third example, we show that XPS can effectively capture the surface oxygen vacancy formation and annihilation during redox cycling. In this experiment [54], XPS was performed on $SnO_{2-\delta}$ subjected to alternating cycles of exposure to ultra-high vacuum (UHV) and O_2 atmospheres. The Sn-to-O ratio of $SnO_{2-\delta}$ was quantified during the redox cycling at 350 °C is shown in Fig. 3c. As illustrated, XPS effectively monitored the variation in oxygen vacancy concentration within $SnO_{2-\delta}$ during this process. Starting with an O/Sn value of around 1.3 after the initial UHV reduction, the ratio increased to approximately 1.7 after exposing the sample to 1 mTorr O_2. The increased O/Sn ratio after O_2 exposure reflects a decrease in oxygen vacancy concentration due to sample oxidation. The subsequent cycle consistently reproduced O/Sn values of ~1.7 under 1 mTorr O_2 and ~1.5 under UHV. Notably, under 2 mTorr O_2 conditions, the O/Sn ratio further increased to approximately 1.8, reflecting a more oxidized sample surface under elevated O_2 pressure. The remarkable reversibility of the quantified O/Sn ratio and its

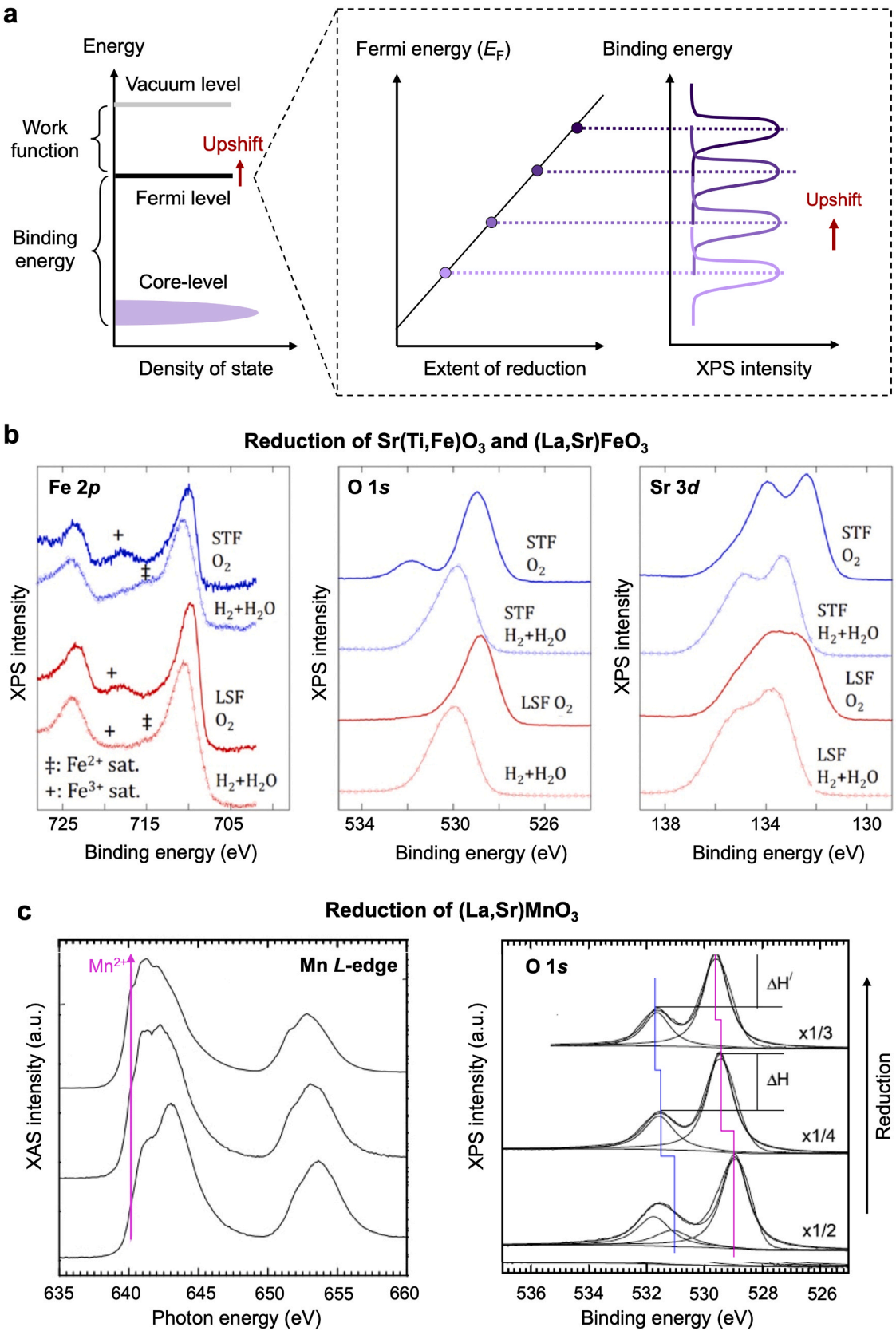

Fig. 4. Oxygen vacancy formation induces electrostatic binding energy shifts in XPS. (a) Schematics depict how variations in Fermi energy can lead to XPS binding energy shifts. (b) Comparison of Fe 2*p*, O 1*s*, and Sr 3*d* spectra between STF and LSF under O_2 and H_2/H_2O atmospheres. The Fe 2*p* spectra clearly indicate sample reduction in H_2/H_2O. More importantly, the binding energy of O and Sr increases by approximately 0.9 eV in a reducing atmosphere. (c) Similarly, the reduction of LSM, evident from Mn L-edge absorption spectra, also leads to a shift in the O 1*s* spectra toward higher binding energy.
(b) Reprinted from Ref. [57] with permission. Copyright 2015 American Chemical Society. (c) Reproduced from Ref. [62] with permission.

high sensitivity to external oxygen partial pressure highlight the reliability of using XPS for the precise quantification of surface oxygen stoichiometry. This example also highlights that even though we cannot directly probe a vacant oxygen site with XPS, we can accurately assess the oxygen vacancy concentration in the sample by precisely quantifying the oxygen stoichiometry.

4. Probing oxygen vacancies via Fermi level shift analysis

Since oxygen vacancy formation in metal oxides is often accompanied by electron doping into the materials [32], the Fermi energy level tends to undergo an upward shift during oxygen vacancy formation [55,56]. This effect can be also investigated using XPS [57,58]. This is because the binding energy represents the energy difference between an occupied electronic state and the Fermi level [59], and an upward shift in the Fermi energy will lead to an apparent increase in binding energy (Fig. 4a). Therefore, the presence of oxygen vacancies can be probed by quantifying electrostatic shifts in binding energies in XPS. It is crucial to acknowledge that variations in the oxidation state can also induce a shift in binding energy [60], known as the "chemical shift.[61]" For example, as shown Fig. 2b, the Ti 2*p* spectra from reduced Ti^{3+} species display a lower binding energy than the oxidized Ti^{4+}. Therefore, a thorough analysis of the redox-inactive spectra is necessary to confirm that the observed binding energy shift is attributed to the formation or annihilation of oxygen vacancies.

Here, we give a few examples on binding energy shift in core-level spectra during the reduction of perovskite oxides. In Fig. 4b, we show the Sr 3*d*, O 1*s*, and Fe 2*p* XPS spectra of LSF and $SrTi_{0.65}Fe_{0.35}O_3$ (STF) under both oxidizing and reducing atmospheres at 615°C (Ref. [57]). The Fe 2*p* spectra reveal a clear reduction in the Fe valence state for both LSF and STF when exposed to the H_2/H_2O atmosphere, characterized by a reduction in the Fe^{3+} satellite features. Throughout this reduction process, Sr^{2+} and O^{2-} remain redox-inactive with a constant valence state. However, the binding energy of the Sr 3*d* and O 1*s* spectra exhibited an approximate 1 eV increase upon transitioning from O_2 to the H_2/H_2O atmospheres. Although not shown in Fig. 4b, the Ti 2*p* and La 4*d* spectra also exhibit similar binding energy shifts during the reduction process for STF and LSF, respectively [57]. As another example, in Fig. 4c, we show the O 1*s* spectral evolution for $La_{0.2}Sr_{0.8}MnO_3$ (LSM) during reduction [62]. The reduction-induced valence state reduction of Mn cations is confirmed with X-ray absorption spectroscopy (XAS). Notably, the O 1*s* spectra also shift towards higher binding energy as LSM undergoes reduction, similar to STF and LSF.

To date, a comprehensive quantitative analysis of oxygen vacancy concentration through electrostatic binding energy shift analysis in XPS spectra has yet to be fully established. This is partially attributed to the challenge of interpreting the somewhat complex binding energy shifts. Nevertheless, we include this approach due to its potential for numerous applications, given the sensitivity of Fermi energy shifts to small changes oxygen vacancy concentrations in certain systems [63]. One viable strategy for XPS binding energy analysis involves integrating it with thermodynamic defect modeling. For example, Rothschild *et al.* developed a defect model for $SrTi_{1-x}Fe_xO_{3-\delta}$ (STF) solid solutions, where they calculated the variation in the Fermi level as a function of the oxygen partial pressure [61]. Their model demonstrated a Fermi level increase of approximately 1 eV when the system changed from oxidizing (10^4 Pa) to reducing (10^{-14} Pa) conditions at 850 °C. Notably, this calculated 1 eV Fermi level shift aligns with the experimentally observed binding energy shift in Fig. 4b. In a separate investigation, Bak *et al.* calculated the Fermi level variation in $(La,Sr)MnO_3$ as a function of oxygen partial pressure [63]. In their study, these authors also revealed a Fermi level upshift upon oxygen vacancy formation, in alignment with the XPS spectral shift shown in Fig. 4c. Therefore, the integration of defect modeling with XPS quantification holds the promise of establishing a quantitative relationship between electrostatic binding energy shifts and oxygen nonstoichiometry in materials.

5. Conclusion

In this work, we discuss three approaches for investigating oxygen vacancies with XPS: (1) quantifying the valence state of redox-active cation spectra, (2) assessing oxygen nonstoichiometry through normalized oxygen spectra, and (3) evaluating Fermi level variations via the electrostatic binding energy shift in redox-inactive spectra. In contrast to the commonly employed method of analyzing the 531–532 eV O 1*s* spectral feature, these three alternative approaches offer increased reliability by evaluating the true "fingerprints" of oxygen vacancies in XPS. We want to emphasize, however, that each of the three approaches works best for different materials, and selecting the appropriate technique requires prior knowledge of the physicochemical and spectroscopic behavior of the material.

To ensure robust data analysis, when possible and applicable, we recommend future studies to incorporate more than one of these three analytical approaches when employing XPS for oxygen vacancy quantification and to evaluate which are applicable. This precaution is crucial because individual phenomena — such as changes in valence state, normalized oxygen intensity reduction, and binding energy shifts — do not inherently imply a change in oxygen vacancy concentration within metal oxides. First, a reduction in cation valence state does not necessarily imply the formation of oxygen vacancies. For instance, protonation can also lead to a decrease in the valence state of cations in oxides, without affecting the total oxygen concentration within the lattice [64]. Second, during the reduction/oxidation process, cation segregation [65] and depletion [47] may occur on the surface. Consequently, observed variations in the surface anion-to-cation ratio may predominantly stem from changes in cation stoichiometry rather than oxygen vacancy concentration. Furthermore, the electrostatic binding energy shift may be induced by surface band bending [66], formation of a space charge layer [67] or sample charging [68,69], introducing a potential source of ambiguity. Therefore, to mitigate the limitations associated with a single analytical method, we recommend analyzing both anion and cation spectra to corroborate the presence and concentration of oxygen vacancies within a material. We anticipate that this multifaceted approach will enhance the robustness and reliability of oxygen vacancy assessments from XPS, thereby deepening our understanding and ability to manipulate oxygen vacancies in materials.

CRediT authorship contribution statement

Jiayue Wang: Writing – review & editing, Writing – original draft, Methodology, Formal analysis, Data curation, Conceptualization. **David N. Mueller:** Writing – review & editing, Conceptualization. **Ethan J. Crumlin:** Writing – review & editing, Writing – original draft, Supervision, Project administration, Methodology, Investigation, Funding acquisition, Formal analysis, Data curation, Conceptualization.

Declaration of Competing Interest

The authors declare that they have no known competing financial interests or personal relationships that could have appeared to influence the work reported in this paper.

Acknowledgements

J.W. was supported by the Gordon and Betty Moore Foundation's Emergent Phenomena in Quantum Systems Initiative (Grant No. GBMF9072, synthesis equipment). E.J.C. was supported by the Condensed Phase and Interfacial Molecular Science Program (CPIMS), in the Chemical Sciences Geosciences and Biosciences Division of the Office of Basic Energy Sciences of the U.S. Department of Energy under Contract No. DE-AC02–05CH11231. D.N.M. gratefully acknowledges

financial support from the German Science Foundation (DFG) in the frame of the priority program "Manipulation of matter controlled by electric and magnetic field: Towards novel synthesis and processing routes of inorganic materials" (SPP 1959) under project MU 4591/1-2.

References

[1] D. Dong, et al., Emerging applications of metal-oxide thin films for flexible and stretchable electronic devices, Appl. Phys. Rev. 10 (2023) 031314, https://doi.org/10.1063/5.0151297.

[2] U. Farooq, T. Ahmad, F. Naaz, S. u Islam, Review on metals and metal oxides in sustainable energy production: progress and perspectives, Energy Fuels 37 (2023) 1577–1632, https://doi.org/10.1021/acs.energyfuels.2c03396.

[3] B. Saruhan, R. Lontio Fomekong, S. Nahirniak, Review: influences of semiconductor metal oxide properties on gas sensing characteristics, Front. Sens. 2 (2021).

[4] G. Pacchioni, Oxygen Vacancy: The Invisible Agent on Oxide Surfaces (https://doi.org:), Chemphyschem 4 (2003) 1041–1047, https://doi.org/10.1002/cphc.200300835.

[5] F. Gunkel, D.V. Christensen, Y.Z. Chen, N. Pryds, Oxygen vacancies: The (in)visible friend of oxide electronics (https://doi.org:), Appl. Phys. Lett. 116 (2020) 120505, https://doi.org/10.1063/1.5143309.

[6] H. Idriss, Oxygen vacancies role in thermally driven and photon driven catalytic reactions, Chem. Catal. 2 (2022) 1549–1560, https://doi.org/10.1016/j.checat.2022.05.022.

[7] Z. Wang, L. Wang, Role of oxygen vacancy in metal oxide based photoelectrochemical water splitting, EcoMat 3 (2021) e12075, https://doi.org/10.1002/eom2.12075.

[8] I. Hussain, et al., A review of the indispensable role of oxygen vacancies for enhanced CO_2 methanation activity over CeO_2-based catalysts: uncovering, influencing, and tuning strategies, Int. J. Hydrog. Energy 48 (2023) 24663–24696, https://doi.org/10.1016/j.ijhydene.2022.08.086.

[9] F. Yan, et al., Recent progress on defect-engineering in ferroelectric HfO_2: the next step forward via multiscale structural optimization, Mater. Horiz. 11 (2024) 626–645, https://doi.org/10.1039/D3MH01273E.

[10] C. Menéndez, D. Chu, C. Cazorla, Oxygen-vacancy induced magnetic phase transitions in multiferroic thin films, npj Comput. Mater. 6 (2020) 76, https://doi.org/10.1038/s41524-020-0344-3.

[11] Y. Li, S. Du, Z.-Y. Weng, Z. Liu, In-plane ordering of oxygen vacancies in a high-Tc cuprate superconductor with compressed Cu-O octahedrons: an automated cluster expansion study, Phys. Rev. Mater. 4 (2020) 044801, https://doi.org/10.1103/PhysRevMaterials.4.044801.

[12] S.J. Skinner, J.A. Kilner, Oxygen ion conductors, Mater. Today 6 (2003) 30–37, https://doi.org/10.1016/S1369-7021(03)00332-8.

[13] S. Hofmann, Auger-and X-ray photoelectron spectroscopy in materials science: a user-oriented guide, Vol. 49, Springer Science & Business Media, 2012.

[14] F.A. Stevie, C.L. Donley, Introduction to x-ray photoelectron spectroscopy (https://doi.org:), J. Vac. Sci. Technol. A 38 (2020) 063204, https://doi.org/10.1116/6.0000412.

[15] G. Greczynski, R.T. Haasch, N. Hellgren, E. Lewin, L. Hultman, X-ray photoelectron spectroscopy of thin films, Nat. Rev. Methods Prim. 3 (2023) 40, https://doi.org/10.1038/s43586-023-00225-y.

[16] Z. Wang, R. Lin, Y. Huo, H. Li, L. Wang, Formation, detection, and function of oxygen vacancy in metal oxides for solar energy conversion, Adv. Funct. Mater. 32 (2022) 2109503, https://doi.org/10.1002/adfm.202109503.

[17] Z. Wang, et al., Understanding the roles of oxygen vacancies in hematite-based photoelectrochemical processes, Angew. Chem. Int. Ed. 58 (2019) 1030–1034, https://doi.org/10.1002/anie.201810583.

[18] D. Chen, et al., Constructing a pathway for mixed ion and electron transfer reactions for O_2 incorporation in $Pr_{0.1}Ce_{0.9}O_{2-x}$, Nat. Catal. (2020), https://doi.org/10.1038/s41929-019-0401-9.

[19] M. Rogala, et al., Self-reduction of the native TiO_2 (110) surface during cooling after thermal annealing – in-operando investigations, Sci. Rep. 9 (2019) 12563, https://doi.org/10.1038/s41598-019-48837-3.

[20] J.P. Holgado, G. Munuera, J.P. Espinós, A.R. González-Elipe, XPS study of oxidation processes of CeO_x defective layers, Appl. Surf. Sci. 158 (2000) 164–171, https://doi.org/10.1016/S0169-4332(99)00597-8.

[21] M.A. Henderson, C.L. Perkins, M.H. Engelhard, S. Thevuthasan, C.H.F. Peden, Redox properties of water on the oxidized and reduced surfaces of CeO_2, Surf. Sci. 526 (111) (2003) 1–18, https://doi.org/10.1016/S0039-6028(02)02657-2.

[22] D.J. Morgan, Photoelectron spectroscopy of ceria: reduction, quantification and the myth of the vacancy peak in XPS analysis, Surf. Interface Anal. 55 (2023) 845–850, https://doi.org/10.1002/sia.7254.

[23] A. Posada-Borbón, N. Bosio, H. Grönbeck, On the signatures of oxygen vacancies in O1s core level shifts, Surf. Sci. 705 (2021) 121761, https://doi.org/10.1016/j.susc.2020.121761.

[24] N. Bosio, A. Schaefer, H. Grönbeck, Can oxygen vacancies in ceria surfaces be measured by O1s photoemission spectroscopy? J. Phys.: Condens. Matter 34 (2022) 174004 https://doi.org/10.1088/1361-648X/ac4f7b.

[25] T.J. Frankcombe, Y. Liu, Interpretation of Oxygen 1s X-ray Photoelectron Spectroscopy of ZnO, Chem. Mater. 35 (2023) 5468–5474, https://doi.org/10.1021/acs.chemmater.3c00801.

[26] H. Idriss, On the wrong assignment of the XPS O1s signal at 531–532 eV attributed to oxygen vacancies in photo- and electro-catalysts for water splitting and other materials applications, Surf. Sci. 712 (2021) 121894, https://doi.org/10.1016/j.susc.2021.121894.

[27] Y. Hinuma, et al., Density functional theory calculations of oxygen vacancy formation and subsequent molecular adsorption on oxide surfaces, J. Phys. Chem. C. 122 (2018) 29435–29444, https://doi.org/10.1021/acs.jpcc.8b11279.

[28] Q. Chen, et al., Observation of oxygen vacancy filling under water vapor in ceramic proton conductors in situ with ambient pressure XPS, Chem. Mater. 25 (2013) 4690–4696, https://doi.org/10.1021/cm401977p.

[29] L.-Q. Wang, D.R. Baer, M.H. Engelhard, A.N. Shultz, The adsorption of liquid and vapor water on TiO_2(110) surfaces: the role of defects, Surf. Sci. 344 (1995) 237–250, https://doi.org/10.1016/0039-6028(95)00859-4.

[30] B. Wang, et al., Adsorption and oxidation of SO_2 on the surface of TiO_2 nanoparticles: the role of terminal hydroxyl and oxygen vacancy–Ti3+ states, Phys. Chem. Chem. Phys. 22 (2020) 9943–9953, https://doi.org/10.1039/D0CP00785D.

[31] M.J. Jackman, A.G. Thomas, C. Muryn, Photoelectron spectroscopy study of stoichiometric and reduced anatase TiO_2(101) surfaces: the effect of subsurface defects on water adsorption at near-ambient pressures, J. Phys. Chem. C. 119 (2015) 13682–13690, https://doi.org/10.1021/acs.jpcc.5b02732.

[32] D.A. Muller, N. Nakagawa, A. Ohtomo, J.L. Grazul, H.Y. Hwang, Atomic-scale imaging of nanoengineered oxygen vacancy profiles in $SrTiO_3$, Nature 430 (2004) 657–661, https://doi.org/10.1038/nature02756.

[33] M. Kuhn, J.J. Kim, S.R. Bishop, H.L. Tuller, Oxygen Nonstoichiometry and Defect Chemistry of Perovskite-Structured $Ba_xSr_{1-x}Ti_{1-y}FeyO_{3-y/2+\delta}$ Solid Solutions, Chem. Mater. 25 (2013) 2970–2975, https://doi.org/10.1021/cm400546z.

[34] R.A. De Souza, D.N. Mueller, Electrochemical methods for determining ionic charge in solids (https://doi.org:), Nat. Mater. 20 (2021) 443–446, https://doi.org/10.1038/s41563-020-0790-9.

[35] A. Walsh, A.A. Sokol, J. Buckeridge, D.O. Scanlon, C.R.A. Catlow, Oxidation states and ionicity (https://doi.org:), Nat. Mater. 17 (2018) 958–964, https://doi.org/10.1038/s41563-018-0165-7.

[36] F. d Groot, Multiplet effects in X-ray spectroscopy (https://doi.org:), Coord. Chem. Rev. 249 (2005) 31–63, https://doi.org/10.1016/j.ccr.2004.03.018.

[37] J. Wang, et al., Threshold catalytic onset of carbon formation on CeO_2 during CO_2 electrolysis: mechanism and inhibition, J. Mater. Chem. A 7 (2019) 15233–15243, https://doi.org/10.1039/C9TA03265G.

[38] G. Silversmit, D. Depla, H. Poelman, G.B. Marin, R. De Gryse, An XPS study on the surface reduction of V_2O_5 (001) induced by Ar+ ion bombardment, Surf. Sci. 600 (2006) 3512–3517, https://doi.org/10.1016/j.susc.2006.07.006.

[39] A.E. Bocquet, et al., Electronic structure of early 3d-transition-metal oxides by analysis of the 2p core-level photoemission spectra, Phys. Rev. B 53 (1996) 1161–1170, https://doi.org/10.1103/PhysRevB.53.1161.

[40] G.H. Major, et al., Practical guide for curve fitting in x-ray photoelectron spectroscopy, J. Vac. Sci. Technol. A 38 (2020) 061203, https://doi.org/10.1116/6.0000377.

[41] A.G. Shard, Practical guides for x-ray photoelectron spectroscopy: Quantitative XPS, J. Vac. Sci. Technol. A 38 (2020) 041201, https://doi.org/10.1116/1.5141395.

[42] C.R. Brundle, B.V. Crist, X-ray photoelectron spectroscopy: A perspective on quantitation accuracy for composition analysis of homogeneous materials, J. Vac. Sci. Technol. A 38 (2020) 041001, https://doi.org/10.1116/1.5143897.

[43] D.N. Mueller, M.L. Machala, H. Bluhm, W.C. Chueh, Redox activity of surface oxygen anions in oxygen-deficient perovskite oxides during electrochemical reactions, Nat. Commun. 6 (2015) 6097, https://doi.org/10.1038/ncomms7097.

[44] J. Wang, et al., Strain-Dependent Surface Defect Equilibria of Mixed Ionic-Electronic Conducting Perovskites, Chem. Mater. 34 (2022) 5138–5150, https://doi.org/10.1021/acs.chemmater.2c00614.

[45] H. Wadati, et al., Hole-doping-induced changes in the electronic structure of $La_{1-x}Sr_xFeO_3$: Soft x-ray photoemission and absorption study of epitaxial thin films (https://doi.org:), Phys. Rev. B 71 (2005) 035108, https://doi.org/10.1103/PhysRevB.71.035108.

[46] M. Abbate, et al., Controlled-valence properties of $La_{1-x}Sr_xFeO_3$ and $La_{1-x}Sr_xMnO_3$ studied by soft-x-ray absorption spectroscopy, Phys. Rev. B 46 (1992) 4511–4519, https://doi.org/10.1103/PhysRevB.46.4511.

[47] J. Wang, et al., Exsolution-driven surface transformation in the host oxide, Nano Lett. 22 (2022) 5401–5408, https://doi.org/10.1021/acs.nanolett.2c01439.

[48] M.L. Weber, et al., Atomistic insights into activation and degradation of $La_{0.6}Sr_{0.4}CoO_{3-\delta}$ electrocatalysts under oxygen evolution conditions, J. Am. Chem. Soc. 144 (2022) 17966–17979, https://doi.org/10.1021/jacs.2c07226.

[49] L.T. Hudson, R.L. Kurtz, S.W. Robey, D. Temple, R.L. Stockbauer, Surface core-level shifts of barium observed in photoemission of vacuum-fractured $BaTiO_3$ (100), Phys. Rev. B 47 (1993) 10832–10838, https://doi.org/10.1103/PhysRevB.47.10832.

[50] J. Wang, et al., Tuning point defects by elastic strain modulates nanoparticle exsolution on perovskite oxides, Chem. Mater. 33 (2021) 5021–5034, https://doi.org/10.1021/acs.chemmater.1c00821.

[51] D. Neagu, et al., Roadmap on exsolution for energy applications, J. Phys.: Energy 5 (2023).

[52] M. Kuhn, S. Hashimoto, K. Sato, K. Yashiro, J. Mizusaki, Oxygen nonstoichiometry, thermo-chemical stability and lattice expansion of $La_{0.6}Sr_{0.4}FeO_{3-\delta}$, Solid State Ion. 195 (2011) 7–15, https://doi.org/10.1016/j.ssi.2011.05.013.

[53] C. Balaji Gopal, et al., Equilibrium oxygen storage capacity of ultrathin $CeO_{2-\delta}$ depends non-monotonically on large biaxial strain, Nat. Commun. 8 (2017) 15360, https://doi.org/10.1038/ncomms15360.

[54] S. Kucharski, et al., Direct in situ spectroscopic evidence of the crucial role played by surface oxygen vacancies in the O_2-sensing mechanism of SnO_2 (https://doi.org:), Chem. Sci. 13 (2022) 6089–6097, https://doi.org/10.1039/D2SC01738E.

[55] A. Rothschild, W. Menesklou, H.L. Tuller, E. Ivers-Tiffée, Electronic structure, defect chemistry, and transport properties of $SrTi_{1-x}Fe_xO_{3-y}$ solid solutions, Chem. Mater. 18 (2006) 3651–3659, https://doi.org/10.1021/cm052803x.
[56] A. Klein, et al., The Fermi energy as common parameter to describe charge compensation mechanisms: a path to Fermi level engineering of oxide electroceramics, J. Electroceram. (2023), https://doi.org/10.1007/s10832-023-00324-y.
[57] A. Nenning, et al., Ambient Pressure XPS study of mixed conducting perovskite-type SOFC cathode and anode materials under well-defined electrochemical polarization, J. Phys. Chem. C. 120 (2016) 1461–1471, https://doi.org/10.1021/acs.jpcc.5b08596.
[58] W.C. Chueh, et al., Highly Enhanced Concentration and Stability of Reactive Ce^{3+} on Doped CeO_2 Surface Revealed In Operando, Chem. Mater. 24 (2012) 1876–1882, https://doi.org/10.1021/cm300574v.
[59] A. Kahn, Fermi level, work function and vacuum level, Mater. Horiz. 3 (2016) 7–10, https://doi.org/10.1039/C5MH00160A.
[60] P.S. Bagus, C.J. Nelin, C.R. Brundle, Chemical significance of x-ray photoelectron spectroscopy binding energy shifts: a perspective, J. Vac. Sci. Technol. A 41 (2023) 068501, https://doi.org/10.1116/6.0003081.
[61] T.C. Taucher, I. Hehn, O.T. Hofmann, M. Zharnikov, E. Zojer, Understanding chemical versus electrostatic shifts in X-ray photoelectron spectra of organic self-assembled monolayers, J. Phys. Chem. C. 120 (2016) 3428–3437, https://doi.org/10.1021/acs.jpcc.5b12387.
[62] J. Zhao, et al., Oxygen vacancy induced electronic structure variation in the $La_{0.2}Sr_{0.8}MnO_3$ thin film, AIP Adv. 9 (2019) 055208, https://doi.org/10.1063/1.5088738.
[63] T. Bak, J. Nowotny, M. Rekas, C.C. Sorrell, Non-stoichiometry, Fermi energy and work function of $(La,Sr)MnO_3$. II. Verification of theoretical model, J. Phys. Chem. Solids 62 (2001) 737–742, https://doi.org/10.1016/S0022-3697(00)00231-6.
[64] X. Yao, et al., Protonic solid-state electrochemical synapse for physical neural networks (https://doi.org:), Nat. Commun. 11 (2020) 3134, https://doi.org/10.1038/s41467-020-16866-6.
[65] E.J. Crumlin, et al., Surface strontium enrichment on highly active perovskites for oxygen electrocatalysis in solid oxide fuel cells (https://doi.org:), Energy Environ. Sci. 5 (2012) 6081–6088, https://doi.org/10.1039/C2EE03397F.
[66] S. Porsgaard, et al., Charge State of Gold Nanoparticles Supported on Titania under Oxygen Pressure, Angew. Chem. Int. Ed. 50 (2011) 2266–2269, https://doi.org/10.1002/anie.201005377.
[67] M. Andrä, et al., Oxygen partial pressure dependence of surface space charge formation in donor-doped $SrTiO_3$, APL Mater. 5 (2017) 056106, https://doi.org/10.1063/1.4983618.
[68] G. Greczynski, L. Hultman, X-ray photoelectron spectroscopy: Towards reliable binding energy referencing, Prog. Mater. Sci. 107 (2020) 100591, https://doi.org/10.1016/j.pmatsci.2019.100591.
[69] D.R. Baer, et al., XPS guide: charge neutralization and binding energy referencing for insulating samples, J. Vac. Sci. Technol. A 38 (2020) 031204, https://doi.org/10.1116/6.0000057.

Jiayue Wang is a postdoctoral scholar at the Geballe Laboratory for Advanced Materials at Stanford University. He received his Ph.D. in nuclear science and engineering from the Massachusetts Institute of Technology in 2022. Prior to that, he obtained his B.E. in engineering physics from Tsinghua University, China. His research focuses on understanding and designing functional atomic defects in electroceramics. In particular, his studies combine advanced thin-film synthesis and ambient pressure X-ray photoelectron spectroscopy (APXPS) to elucidate point defect chemistry at redox-active interfaces, such as those involved in phase transformations and catalytic reactions.

David N. Mueller is a staff scientist at the Peter Gruenberg Institute of the Research Centre Juelich, Germany. He received his PhD in physical chemistry from RWTH Aachen University, Germany in 2010 on the topic of mixed conducting perovskite oxides for oxygen separation membranes where he was first exposed to in situ X-Ray spectroscopies. In 2012 he moved to Stanford University, CA, as a postdoctoral scholar in the department of materials science and engineering, focusing on in situ and operando X-Ray spectroscopies on mixed conducting oxides for energy conversion devices. Since 2015 he is part of the Peter Gruenberg Institute with his main focus on utilization of X-ray spectroscopic and microscopic techniques to assess fundamental physicochemical concepts and processes in materials science.

Ethan J. Crumlin is a staff scientist at the Lawrence Berkeley National Laboratory (LBNL), USA. He received his PhD in mechanical engineering from Massachusetts Institute of Technology, USA, in 2012 on high-temperature electrocatalysis, where he discovered *in situ* and *operando* APXPS. Since then, he joined LBNL as a postdoctoral fellow and then as a scientist at the Advanced Light Source (ALS), specializing in *operando* APXPS of (electro)catalysis at the solid/gas and solid/liquid interface. He has become the APXPS & Chemical Sciences Program Lead at ALS, and in 2023, LBNL's Deputy Director for the Chemical Sciences Division.